Translational Oncology 43 (2024) 101910

Contents lists available at ScienceDirect

Translational Oncology

journal homepage: www.elsevier.com/locate/tranon

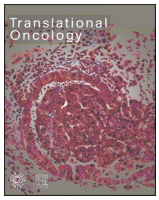

Original Research

Prediction of immunotherapy responsiveness in melanoma through single-cell sequencing-based characterization of the tumor immune microenvironment

Yucheng Dong [a,1], Zhizhuo Chen [a,1], Fan Yang [b], Jiaxin Wei [c], Jiuzuo Huang [a,*], Xiao Long [a,*]

[a] Peking Union Medical College Hospital, Chinese Academy of Medical Sciences & Peking Union Medical College, Beijing 100730, China
[b] Department of Liver Surgery, Peking Union Medical College Hospital, Chinese Academy of Medical Sciences & Peking Union Medical College, Beijing, China
[c] Department of Emergency Department, Peking Union Medical College Hospital, Chinese Academy of Medical Sciences & Peking Union Medical College, Beijing, China

ARTICLE INFO

Keywords:
Immunotherapy
Machine learning
Melanoma
Single-cell sequencing
Tumor micro-environment

ABSTRACT

Immune checkpoint inhibitors (ICB) therapy have emerged as effective treatments for melanomas. However, the response of melanoma patients to ICB has been highly heterogenous. Here, by analyzing integrated scRNA-seq datasets from melanoma patients, we revealed significant differences in the TiME composition between ICB-resistant and responsive tissues, with resistant or responsive tissues characterized by an abundance of myeloid cells and CD8+ *T* cells or CD4+ *T* cell predominance, respectively. Among CD4+ *T* cells, CD4+ CXCL13+ Tfh-like cells were associated with an immunosuppressive phenotype linked to immune escape-related genes and negative regulation of T cell activation. We also develop an immunotherapy response prediction model based on the composition of the immune compartment. Our predictive model was validated using CIBERSORTx on bulk RNA-seq datasets from melanoma patients pre- and post-ICB treatment and showed a better performance than other existing models. Our study presents an effective immunotherapy response prediction model with potential for further translation, as well as underscores the critical role of the TiME in influencing the response of melanomas to immunotherapy.

Introduction

Melanoma, a malignant skin cancer originating from melanocytes, has been of immense clinical interest due to its aggressive nature and limited therapeutic options [1]. Recently, immunotherapies, particularly immune checkpoint inhibitors (ICB), including anti-PD-1/PD-L1 or anti-CTLA-4 therapies [2], have emerged as promising strategies for managing melanoma [3,4]. However, while immunotherapy has showed remarkable efficacy in some patients, the wide variability in anti-tumor responses to this mode of therapy as well as the observation of acquired resistance in nearly half of ICB-treated patients [5] have elicited great interest in developing patient-stratification tools for identifying those who would benefit most from ICB treatment [6–9]. Numerous biomarkers, such as PD-L1 expression [10], tumor mutation burden (TMB) [11], and microsatellite instability [12] have been clinically for assessing responses to PD-1/PD-L1 inhibitors. However, the accuracy of these biomarkers remains limited, as they exhibit significant variations in predictive efficacy across different patient populations [13]. Previous studies suggested that peripheral-derived T cells, such as specific subpopulations of memory CD4+ or CD8+ *T* cells, may correlate with ICB treatment response [14–17]. However, few of these studies have demonstrate their efficacy on a validation cohort. Consequently, to-date, current biomarkers for stratifying ICB-responders from non-responders for melanoma patients need to be further improved for better predictive efficacy.

To optimize the implementation of immunotherapeutic treatment for melanoma patients, we must develop a clinically viable and highly accurate predictive model of response. Immune components in the tumor immune microenvironment (TiME), which have been shown to mediate response to therapeutic interventions [18], have recently emerged as potential factors for predicting patient responses to immunotherapy [19,20]. Indeed, interactions between the host's immune cells (e.g. T cells, B

Abbreviations: ICB, immune checkpoint blockade; ROC, receiver operating characteristic; TiME, the tumor immune microenvironment; Tfh, T follicular helper.

* Corresponding authors.
E-mail addresses: hjz1983@126.com (J. Huang), pumclongxiao@126.com (X. Long).

[1] Yucheng Dong and Zhizhuo Chen have contributed equally to this work.

https://doi.org/10.1016/j.tranon.2024.101910
Received 27 November 2023; Received in revised form 13 January 2024; Accepted 8 February 2024

cells, and myeloid cells) and tumor cells as well as the abundance of specific immune consitutents (e.g. immune cell types, cytokines) within the TiMe have been shown to determine responses to treatment [21,22]. Tumor-Reactive CD8+ *T* cells [23], IRX3-high T cell [24], LAG3-high NK cell [25] have been associated with melanoma immunotherapy responsiveness, but few study has incorporated all the immune cells in the TiME for the prediction of responsiveness. Further, recent advances in single-cell transcriptome sequencing (scRNA-seq) have enabled researchers to gain unprecedented insights into the heterogeneity and dynamics of the TiME of solid tumors [26].

Here, we develop a predictive model for identifying melanoma patients who may be responsive to ICB intervention by leveraging public single-cell RNA sequencing (scRNA-seq) datasets of the melanoma TiME from patients with varying responses to ICB. Upon annotating the immune cell subtypes in the three scRNA-seq databases, we identified distinct differences, including within the T cell compartment, between ICB-responsive and non-responsive melanomas and highlighted the CD4-CXCL13-Tfh cells as an important player in the TiME, which has not been reported in melanoma before. Initially, based on these findings, we leveraged the association between T cell subset and type of response to define a T score to predict response to immunotherapy, but found the predictive power of this model to be limited. To address this challenge, we incorporated qualitative and functional data on all immune constituents within the melanoma TiME into a random forest model, which demonstrated robust predictive capacity when tested on three independent transcriptomic datasets from melanoma patients prior to being treated with ICB. We also compare the performance of our model with existing models, and the result shows our model has an accuracy higher or equal to existing models, highlighting the efficacy of our model. Overall, by incorporating data capturing the dynamics among all immune components within the melanoma TiME, we were able to develop an accurate and precise predictive model to enable the implementation of personalized immunotherapeutic treatments for melanoma patients.

Methods

Obtaining scRNA-seq from melanoma ICI cohorts

To capture the complexity of the melanoma TiME from patients who had received immunotherapy, we obtained the following single-cell transcriptome sequencing datasets from melanoma patients who exhibited differing responses to immunotherapy: (GSE72056 [27], GSE115978 [28], GSE120575 [29]). Patient responses were categorized based on RECIST criteria v1.1 [30], in which complete response (CR) and partial response (PR) were classified as responsive ($n = 15$), while progressive disease (PD) and stable disease (SD) were classified as resistant ($n = 49$). The response rates of patients receiving PD-1 or CTLA-4+PD-1 are similar (**Supplementary Fig. 1C**).

Single-cell transcriptomics analysis

Analysis of single-cell transcriptome data was performed using the Seurat package [31] in R and the Scanpy package [32] in Python. Cells with mitochrondia gene fraction > 10% were filtered out. Unwanted variations and low-quality cells were further filtered by removing cells with high and low (>6000 and <200) expressed features. For single-cell transcriptome data from the three datasets, we first integrated the data using Seurat's "anchors" method [31] and selected cells expressing *PTPRC* (CD45) for subsequent analysis. After normalizing gene expression, we conducted principal component analysis (PCA) for feature extraction and data denoising. We then utilized the Harmony algorithm [33] to remove batch effects, and applied uniform manifold approximation and projection (UMAP) to visualize cells in a two-dimensional space. For dimension-reduced data, we performed Louvain clustering [34] of all immune cells (resolution=0.5) and labeled coarse cell types (e.g. CD8+ *T* cells, CD4+ *T* cells, myeloid cells, etc.). Finally, to provide a highly detailed functional characterization of the TiME, we carried out secondary clustering of T cells, myeloid cells, and B cells (resolution=1) and labeled each subpopulation based on marker genes.

For differential analyzes, genes with a log-fold change (logFC) > 0.25 and a false discovery rate (FDR) < 1e−05 were considered differentially up-regulated, and genes with a logFC_< 0.25 and FDR_< 1e−05 were considered differentially downregulated.

Obtaining bulk RNA-seq data from melanoma ICI cohorts

To validate the efficacy of our model, we obtained bulk RNA-seq data from three datasets that included pre- and post-ICB treatment data from 28 [35], 83 [36], and 51 [37] melanoma patients. Patient responses to immunotherapy were determined using RECIST v 1.1 [30] or immune-related RECIST (irRECIST) [38] criteria, in which CR and PR indicated responsiveness, and PD and SD signified resistance.

Pseudotime analysis

Single-cell pseudotime trajectories were performed using partition-based graph abstraction (PAGA) [39]. Briefly, PAGA infers low dimensional representations of cell clusters by estimating connectivity of high dimensional manifold partitions. To order cells along a trajectory, diffusion-pseudotime (DPT) analysis was implemented and diffusion maps were generated using Scanpy with default parameters. We utilized the Tredeseq package [40] in R to fit and cluster differentially expressed genes along different paths (e.g., *CXCR5, FOXP3*).

Pathway analysis

To assess pathway activity in different subpopulations, we employed gene ontology (GO) analysis using gene sets from the MsigDB [41]. Pathway activity scores were assigned to each cell using Python's decoupler (version=1.5.0) [42] with multivariate linear model. We used unpaired two-sided Student's *t*-tests to analyze differences in pathway activity, with an adjusted p-value < 1e−05 (Benjamini-Hochberg method) indicating significantly differentially activated pathways.

Cell-cell interactions

To identify potential interactions between T cell and myeloid cell clusters, we used the CellCall database [43], which contains a curated repository of interactions between ligand receptors and transcription factors as well as a statistical framework for inferring lineage-specific interactions [44].

Deconvolution algorithm

We utilized the CIBERSORTx algorithm [45] for the deconvolution of bulk RNA-seq data. First, we uploaded the 36 defined immune cell subtypes from our single-cell transcriptome dataset to the CIBERSORTx database and used the "Create Signature Matrix" module to construct signature genes for each cell subtype. Subsequently, we used the "Impute Cell Fractions" module separately on each of the three bulk RNA transcriptome datasets to calculate the relative proportions of the 36 immune cell subtypes.

T score construction

We constructed T scores using the logistic regression function (LogisticRegression) from the Scikit-learn package [46] in Python. The model input variables consisted of the proportions of all T cell subtypes, while the output variable was patient responsiveness to immunotherapy. We allocated 70% of the single-cell transcriptome data as training data ($N = 69$) and the remaining 30% as validation data ($N = 30$). To ensure capturing the most important features, we set the L1

penalty to 0.5. For the deconvolved bulk RNA dataset, we compared T scores between responsive and resistant patients.

Prediction model based on all cell subtypes

To further enhance predictive performance, we used the proportions of all immune cell subtypes in the model to predict patient responsiveness. We allocated 70% of the single-cell transcriptome data ($n = 44$) as training data and the remaining 30% ($n = 20$) as validation data, with the same random seed as for T score construction. We employed logistic regression [47], support vector machines [48], and naïve Bayes [49], gradient boost machine [50] and random forest [51] approaches from the Scikit-learn package to construct predictive models based on the training data and evaluated model performance using the validation data. The random forest model with the best predictive performance was selected as the final predictive model. We utilized the deconvolved bulk RNA sequencing data as an external validation dataset and computed the ROC-AUC for this model on various independent external datasets. To address class imbalance, we employed data augmentation [52] techniques during training to balance the number of resistant and responsive patients.

Results

Single cell immune landscape of immune ICB-Treated melanoma patients

To dissect the TiME of melanoma samples from patients with varying responses (responsive, resistant, unknown) to immune checkpoint therapy, we integrated and analyzed three single-cell transcriptome sequencing datasets of melanoma, including samples pre- and post-immunotherapy **(**Fig. 1**A)**. After implementing quality control measures, 21,586 immune cells (marked by *PTPRC* expression) from 97 samples were identified for subsequent data analysis and, upon further quality control filtering, data integration, and clustering, 19 cell clusters were detected to be further classified into 6 major cell lineages. These cell lineages included myeloid cells (10.49% of total cells; marked by *AIF1* and *LYZ* expression), CD4+ *T* cells (28.40% of total cells; marked by *CD3D, CD3E*, and *CD4* expression), CD8+ *T* cells (39.49% of total cells; marked by *CD3D, CD3E*, and *CD8A* expression), natural killer (NK) cells (7.17% of total cells; marked by *KLRK1* and *NCR1* expression), B cells (12.51% of total cells; marked by *CD79A* expression), and plasma cells (1.94% of total cells; marked by CD79A and CD38 expression) **(**Fig. 1**B and E)**. Subgroup analysis and clustering further divided the 6 major cell lineages into 38 distinct functional subclusters, including CD4+ CXCL13+ *T* Cells and CD8+ PDCD1+ *T* cells **(**Fig. 1**E)**. These findings were validated using bulk transcriptome data, for which we constructed a signature based on the cell clustering classification using CIBERSORTx [53] for predicting its cellular proportions.

We next determined the proportions of the 6 cell lineages identified from our scRNA-seq data in melanoma patients with differential response profiles to immune checkpoint inhibitor treatment, and found that composition of the immune compartment differed between resistant and responsive melanoma tissues **(**Fig. 1**C and D)**. Specifically, resistant tissues harbored an increased proportion of myeloid cells and CD8+ *T* cells, whereas the responsive tissues harbored an increase in CD4+ *T* cells (Fig. 1**C and D**). These findings were was further supported by kernel density estimation, affirming that resistant melanoma tissues harbored constituents that enabled CD8+ *T* cell immunity, while responsive tissues harbored elements that enabled CD4+ *T* cell immunity **(**Fig. 1**F and G)**.

Interestingly, the most substantial difference in the immune compartment between resistant and responsive tissues was observed in the T cell population, thus suggesting that T cells undergo significant changes in response to ICB treatment (Fig. 1**C and D**). To better understand the impact of these differences on response to immunotherapy, we analyzed and compared the overall activity of T cells isolated from resistant and responsive tumors using transcriptomics and gene ontology (GO) analysis. Gene ontology analysis showed that negative regulation of lymphocyte activation and innate immune response pathways were enriched in T cells from both resistant and responsive tumors **(Supplementary Fig. 1A and 1B)**. Overall, our findings suggest that the immune activity of tumoral T cells may contribute to determining response or resistance to immunotherapy in melanomas.

CD4+ CXCL13+ follicular helper-like T cells (Tfh-like) serve as an alternative to regulatory T cells (Treg) and contribute to the resistant phenotype

As T cells are major targets of ICB therapy, as well as are known to undergo significant changes during treatment [54,55], we sought to gain a better understanding of differences in the T cell compartments of melanomas that are responsive or resistant to ICB. Utilizing unsupervised clustering on all T cells, we identified 14 heterogeneous subclusters **(**Figs. 1**E and** 2**A)**. By assessing for the aforementioned signature genes and calculating their average log-transfromed expression level as functional scores, we observed distinct functional status for each CD4+ *T* cell subcluster, with CD4+ FOXP3+ Tregs exhibiting the highest regulatory score and CD4+ CCR7+ IL7R+ *T* cells displaying the highest naive score [56] **(**Fig. 2**C and D)**. Intriguingly, when to those from responsive melanomas, we observed a higher regulatory score in T cells from resistant melanomas (**Supplementary Fig. 2**), indicating a more immunosuppressive phenotype in resistant tumors. In contrast, there was no significant difference in the CD4-FOXP3 Treg fraction between responsive and resistant melanomas **(**Fig. 2**B)**, which aligns with previous studies suggesting that peripheral-derived Treg cells with low regulatory function replenish and infiltrate melanoma tissue during ICB therapy [17,57,6]. Together, these findings suggest that specific CD4+ *T* cell subclusters, distinct from Tregs, may play a crucial role in contributing to the resistant phenotype.

Next, we examined and compared changes in the proportions of each CD4+ *T* cell subcluster in response to ICB in responsive and resistant melanomas. In comparison to that in responsive tumors, we observed a significant expansion of CD4+ CXCL13+ Tfh-like cells in the T cell compartment of resistant tumors when compared to responsive ones ($p = 0.0228$) **(**Fig. 2**B).** Notably, cytotoxic T cell exhaustion and the expression of immune escape-related genes [58,59], such as *TNFRSF4* and *CXCL13*, were found to be upregulated in CD4+ CXCL13+ Tfh-like cells (Fig. 2**G**), and this upregulation has been correlated with poor prognosis in various cancer types [60,61].

Furthermore, GO analysis revealed that genes associated with the regulation of T cell activation were enriched in CD4+ CXCL13+ Tfh-like cells **(Supplementary Fig. 3A)**. These results collectively suggest that CD4+ CXCL13+ Tfh-like cells play an immunosuppressive role in the tumor microenvironment of melanomas resistant to ICB.

To delineate the stages of CD4+ CXCL13+ Tfh-like cells in CD4+ *T* cell differentiation, we performed PAGA trajectory analysis on CD4+ *T* cells with the assumption that CD4+ CCR7+ IL7R+ *T* cells with the highest naïve score served as the starting point for differentiation [62]. Remarkably, CD4+ CXCL13+ Tfh-like cells exhibited a close functional status to both CD4+ FOXP3+ Tregs and CD4+ CXCR5+ Tfh-like cells **(**Fig. 2**E)**, suggesting that CD4+ CXCL13+ Tfh-like cells have the potential to differentiate into either of these subclusters. These findings were further validated using Pearson correlation analysis based on gene expression profiles, which confirmed that the gene expression profile of CD4+ CXCL13+ Tfh-like was similar to that of CD4+ FOXP3+ Tregs (Fig. 2**F**). We next sought to characterize the two potential differentiation trajectories CD4+ CXCL13+ Tfh-like cells (Fig. 2**E**), henceforth referred as the FOXP3+ or CXCR5+ paths. Trajectory-based gene clustering analysis (see Methods for psuedotime analysis) revealed that upregulated GO pathways in the FOXP3+ path primarily involved T cell exhaustion, while pathways upregulated in the CXCR5+ path were primarily associated with antitumoral immunity (**Supplementary**

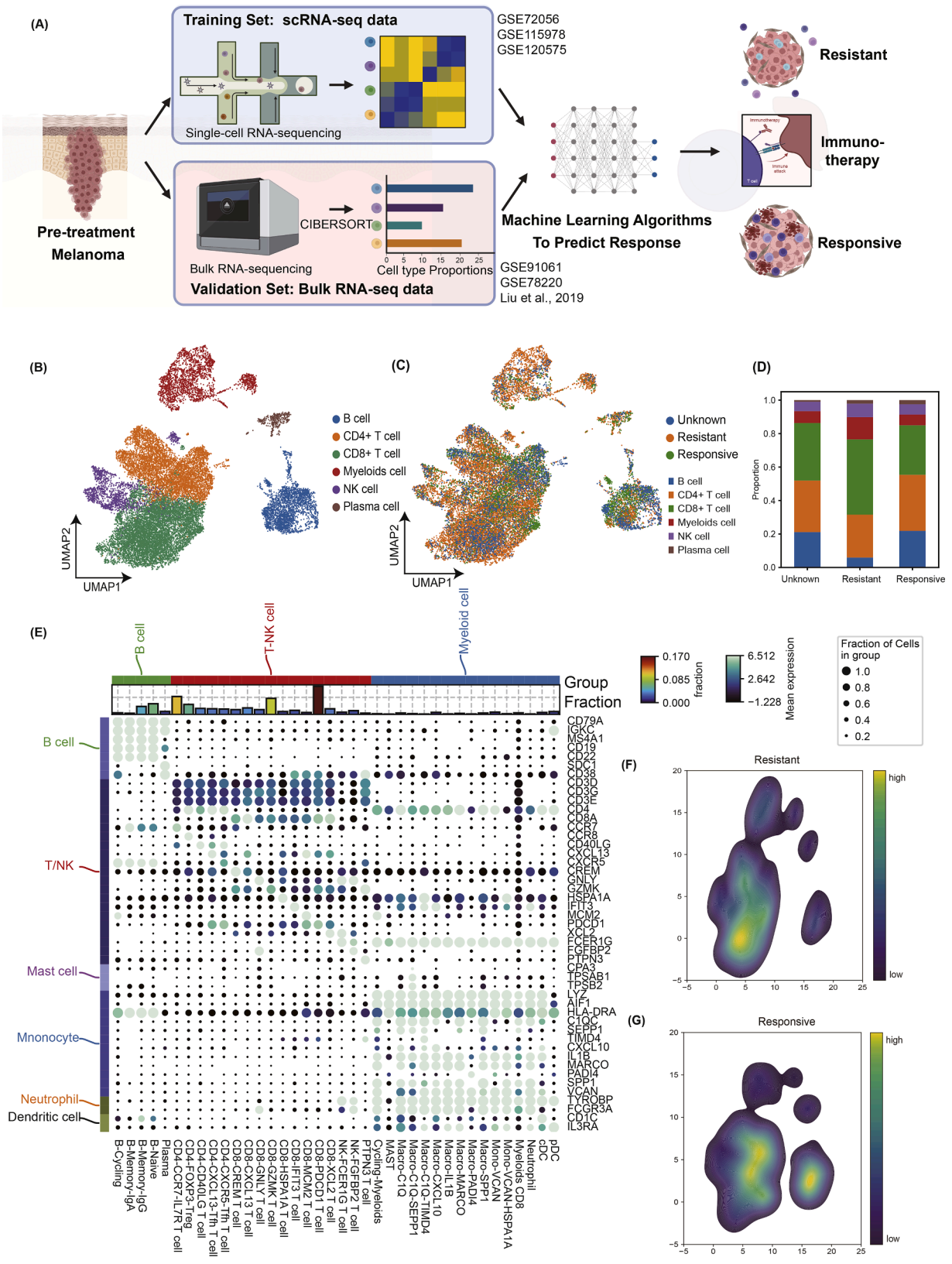

Fig 1. Integrated single-cell RNA-seq reveals transcriptomic heterogeneity of melanoma patients before and after Immune checkpoint blockade therapy. (A) Workflow diagram showing our study to involve the construction of a predictive model for the response of melanoma patients to immunotherapy using three single-cell RNA datasets as the training set and three bulk RNA transcriptome datasets as the validation set. (B) Unbiased clustering of 24,062 cells reveals 6 main immune cellular clusters. Clusters are distinguished by different colors. (C) TSNE plot shows heterogeneity of cell composition for each condition. D) Graph indicating the proportion of cell clusters, defined in legend for (C), in tumor tissue for each condition. (E) Top, bar graph indicating cell sub-clusters and cell-type fractions. Bottom, dot plot showing expression patterns of 46 marker genes for 38 fine annotated cell clusters. (F and G) Kernal density estimation of immune cells in resistant (F) and responsive (G) melanoma patients. Cell Distribution can be referred from Fig. 1C.

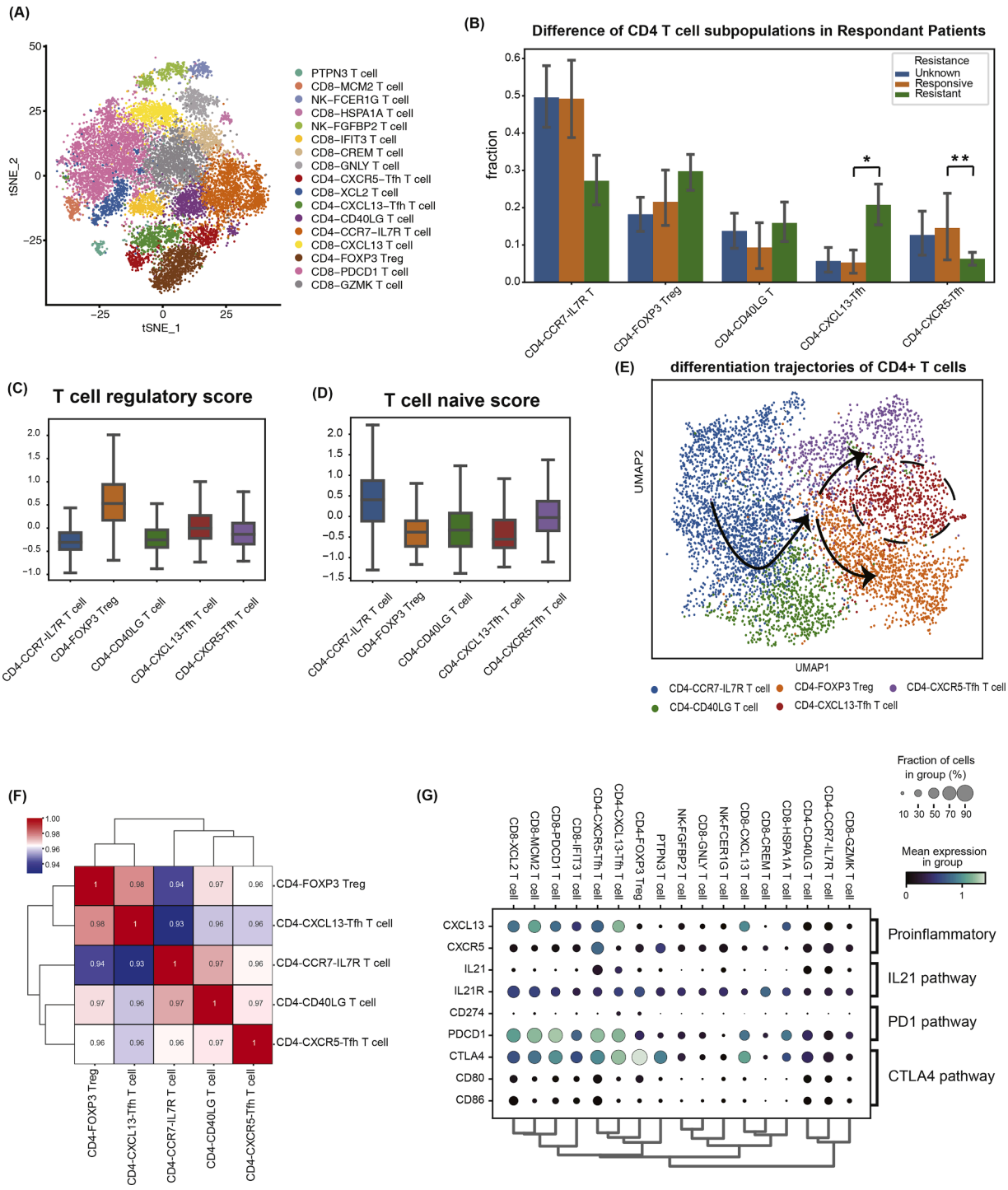

Fig 2. T cells in melanomas cluster into distinct cell populations and CD4+ CXCL13+ follicular helper T cells are increased in immunotherapy-resistant patients. (A) Subclustering of immunotherapy resistant, responsive, and treatment-naïve T-NK cells (cells from CD8+ *T* cell, CD4+ *T* cell, and NK cell shown in Fig. 1) further separated into 17 distinct subtypes. (B) Box plot shows heterogeneity of CD4+ *T* cell composition for each condition. Data analyzed by unpaired two-sided Student's *t*-tests *, $p<0.05$; **, $p<0.01$. Mean +/- SE are shown. (C and D) Box plot show regulatory (C) (calculated with XXXX genes) and naïve (D) (calculated with XXXX genes) T cell scores across CD4+ *T* cell subclusters. Box plots show the quartiles and whiskers show the rest of the score distribution. (E) Pseudotime analysis with PAGA distinguished two potential fates for CD4+ CXCL13+ follicular helper T (tfh) cells. Arrows across the diffusion-pseudotime: Path1 (upper, CXCR5+ *T* cell fate), Path2 (lower CCR8+ *T* cell fate). The general identity of each cell cluster is shown on the bottom. (F) Correlation matrix of gene expression in different CD4+ *T* cell subpopulations. CD4-CXCL13 Tfh-like cells show a strong correlation with CD4-CCR8 T cells and CD4-CXCR5 Tfh-like cells. (G) Dot clustermap shows gene expression patterns of *PD1* and *CTLA4* pathways as well as secreted cytokines across T cell subclusters.

Fig. 3B) [63,64]. Together, these findings suggest that CD4+ CXCL13+ Tfh-like cells may serve as an alternative to Tregs during ICB treatment, thus potentially becoming a valuable prognostic marker for melanoma patients considering ICB treatment.

Developing a melanoma immunotherapy response predictor based on T cell composition

We have previously shown that the composition of the T cell

compartment in ICB-resistant melanomas significantly differs from that in ICB-responsive melanomas (Fig 2**B**). To test whether these differences can be leveraged to predict patient response to immunotherapy, we employed a logistic regression model to construct an immunotherapy response prediction model based on T cell proportions (See Methods). This model uses the proportion of each T cell subpopulation among all immune cells (the count of each T cell subpopulation divided by total immune cell number) as input features, and responses to immunotherapy of each patient as the outputs. To enhance the robustness of the model, we introduced L1 constraints [65] to reduce the number of features that predictive model relies on. The predictive values generated by this model are denoted as 'T scores,' expressed as follows (Fig. 3**A**):

$$\begin{aligned} T\ score = \ & -0.504 \times Prop(CD4-CCR7-IL7R\ T\ cell) + 0.831 \\ & \times Prop(CD4-CXCL13-Tfh\ T\ cell) + -0.768 \\ & \times Prop(CD8-CXCL13\ T\ cell) + 2.0482 \\ & \times Prop(CD8-PDCD1\ T\ cell) \end{aligned}$$

A higher T score indicates that the melanoma has a higher likelihood to exhibit resistance to immunotherapy. In this equation, CD8-PDCD1 T cells have the highest weight and are positively associated with the T score due to the fact that PDCD1 is a therapeutic target of immunotherapy and that the CD8-PDCD1 T cell subtype has been shown to play a primary role in mediating tumor cell cytotoxicity [66,67]. Notably, the highest-weighted cell subtype within CD4+ *T* cells is CD4-CXCL13 Tfh-like cells, for which we (Fig 2**B, A**) and other studies [68] have shown to potentially contribute to inhibiting the effectiveness of immune therapy. Upon calculating T scores for all melanoma patients, our findings revealed significantly higher T scores for ICB-resistant melanomas compared to that for ICB-responsive melanomas (p = 4.6e-03, Fig. 3**B**).

Further, the classification model accurately predicted the prognosis of melanoma patients that have not been treated with ICB (ROC-AUC=0.74, Fig. 3**C**). Because the training dataset for single-cell data included melanoma patients who had been treated with ICB, a model constructed from these data may not be directly applicable to melanoma patients who have not yet been treated with ICB. To assess the model's predictive performance in treatment-naive patients, we tested its efficacy using three independent transcriptomic datasets, each comprising of bulk RNA-seq data from 28 [35], 83 [36], and 51 [37] melanoma patients pre- and post-ICB treatment. Using the signature based on 36 cell subtypes constructed from the single-cell dataset, we estimated the proportions of different cell types within each sample and calculated T scores based on the four T cell components mentioned above (CD4-CCR7-IL7R, CD4-CXCL13-Tfh, CD8-CXCL13, CD8-PDCD1 T cells). Our results showed that ICB-resistant melanomas tended to have higher T scores than ICB-responsive melanomas, although statistical significance was not always observed (p = 0.32, 0.13, 0.03 for each of the three datasets) (Fig. 3**D–F**). This finding suggests that our logistic regression model has the potential to predict response to immunotherapy within certain limitations.

Developing a prediction model based on the proportions of all immune cell types

Considering that high complexity of the TiME in melanomas extend beyond the T cell compartment [69,70], we sought to improve our predictive modeling efforts by comparing the relative proportions of

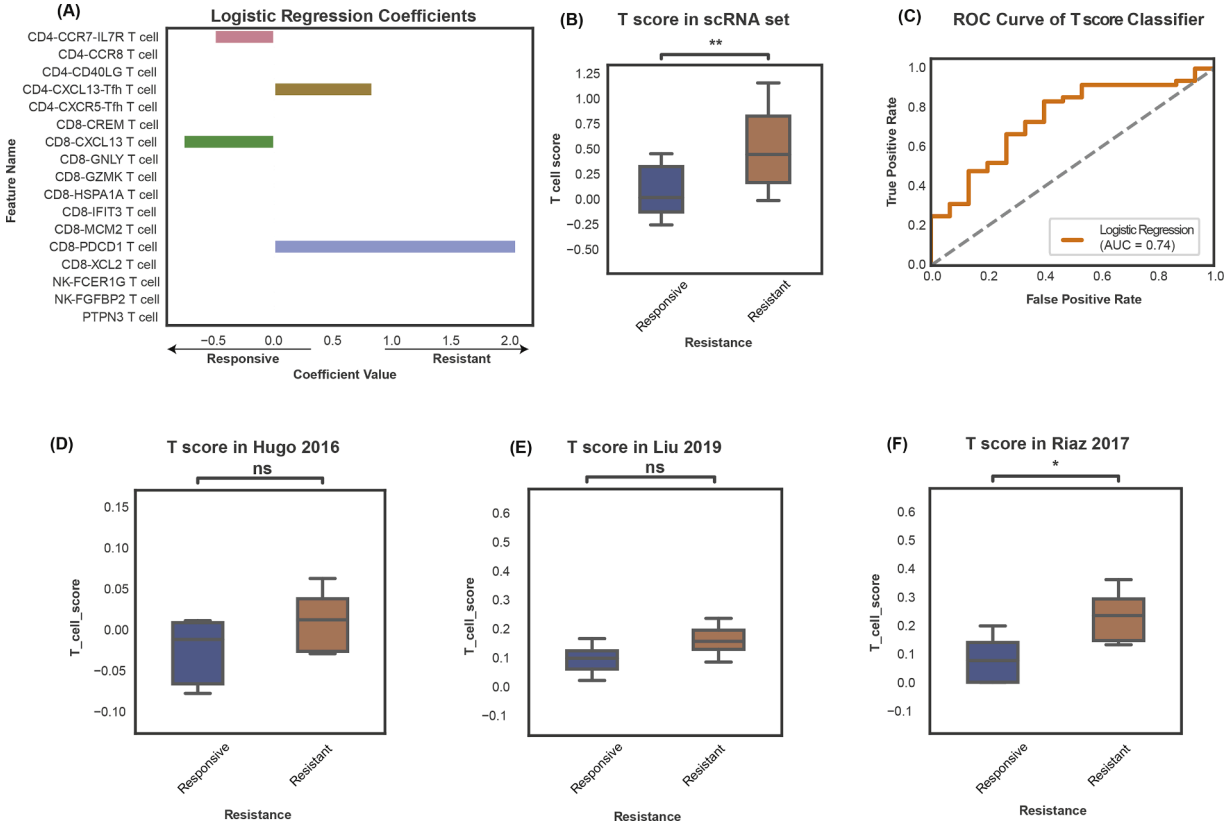

Fig 3. Construction of the predictive model T score based on T cell composition. (A) Coefficients of T cell subpopulations in logistic regression model reflect the importance of each subpopulation in the model. (B) Comparison of T scores between immunotherapy-resistant and -responsive melanomas from the three single-cell sequencing datasets. Data analyzed by unpaired two-sided Student's *t*-tests. p = 4.6e-03. (C) Receiver operating characteristic (ROC) curve of the T score in the training set composed of pre-treatment patients, n = 20. (C-F) Comparison of T scores between immunotherapy-resistant and -responsive melanomas in three independent bulk RNA-seq datasets. Box-and-whisker plots show T score calculated in responsive and resistance patients in each dataset. Data analyzed by unpaired two-sided Student's *t*-tests. *, p<0.05.

functionally defined immune cell subtypes from the single-cell dataset of melanoma patients with different responses to ICB (Figs. 1**E and** 4**A**). Our results revealed an enrichment of PADI4+ Macrophage, CD8-GZMK T cells, and CD8-CXCL13 T cells in ICB-responsive melanomas, while cell types such as CD4-CXCL13 Tfh-like cells and VCAN—HSPA1A+ Mono were enriched in ICB-resistant melanomas. Previous studies have suggested that PADI4 can promote M1 polarization of macrophages, enabling an inflammatory environment that activates immune cells for tumor cell killing [71]. CD8 T cells with high *GZMK* expression act as cytotoxic CD8 effector T cells, capable of directly exerting cytotoxic

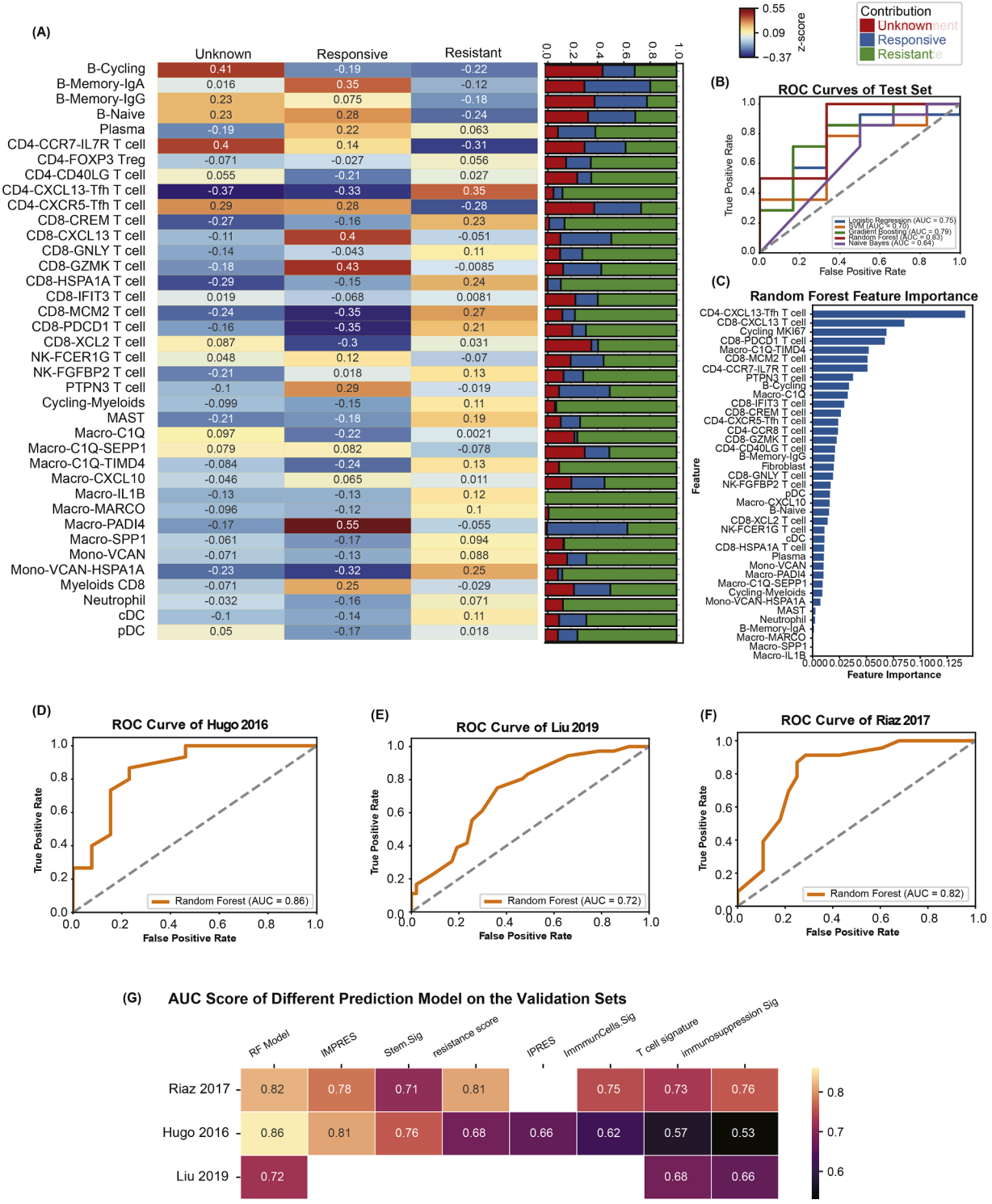

Fig 4. Integrated machine learning models predict patients' response before immunotherapy. (A) Heatmap showing scaled cell fractions used for training the machine learning model. Left, contribution of each condition to the specific cell type. Right, … (B) Receiver operating characteristic (ROC) curves of the integrated machine learning model predicting risk of resistance to immunotherapy in the test set, $n = 20$ individuals. Machine learning algorithms: logistic regression, support vector machines (SVM), random forest, naïve bayes. (C) Feature importance scores obtained from the random forest model. (D-F) ROC curve of the same model on external testing cohort. $n = 28$ (D), 83 (E), 51 (F) individuals. (G) Comparisons of the AUC score calculated by different prediction models on the validation sets. The number in the box indicates ROC-AUC score. The Blank indicates that there is no available result for corresponding model and dataset.

effects on tumor cells [72]. Furthermore, studies have shown that CD8+ *T* cells with high *CXCL13* expression are associated with response to immunotherapy and improved prognosis in patients with multiple cancer types [73].

To describe the predictive roles of different immune cell subtypes on patient response, we employed multiple machine learning methods to construct prediction models. The single-cell dataset was divided into a training set ($n = 44$) and a validation set ($n = 20$). For the training set, we constructed models using simple models including logistic regression [47], support vector machines [48], and naïve Bayes [49], as well as relatively more ensembled models such as gradient boost machine [50] and random forest [51]. We then calculated the ROC-AUC on the validation set and found that the random forest model had the best predictive performance (AUC=0.83, Fig. 4**B**). To validate whether the model is effective for different immunotherapy regimens, we compared its performance in predicting responses for patients treated with PD-1 alone and those treated with CTLA4+PD1, using the original dataset. The results suggest that the model can accurately predict responses for both types of patients (AUC = 0.88 for PD-1, 0.83 for CTLA-4+PD-1, **Supplementary Fig. 4**). Further analysis of the weights assigned to different cell types in the random forest model revealed that CD4-CXCL13 Tfh-like cells and CD8-CXCL13 T cells were the two most critical features (Fig. 4**C**). The pivotal roles of these cell types in mediating response to immunotherapy have been extensively described in literature [68,73,74], thus highlighting the effectiveness of our model.

To assess the generalizability of our predictive random forest model, we tested its predictive capability using three previously described bulk transcriptome datasets. These datasets were subjected to CIBERSORTx deconvolution to estimate the composition of every immune cell subpopulations. Our results demonstrated that random forest model exhibited strong predictive performance in the three independent datasets (ROC-AUC=0.86, 0.72, and 0.82 for each dataset). These findings suggest that the composition of the TiME of treatment-naive patients is capable of predicting immune therapy efficacy to some extent, as well as demonstrate the broad applicability and translational potential of our random forest model. We further compared our random forest model with other melanoma immune therapy response prediction models developed based on transcriptome data in terms of predictive accuracy, measured by ROC-AUC score (Fig. 4**G**). The results indicate that our model's ROC-AUC on the three validation datasets is higher than or the same as most of existing prediction models, including IMPRES [75], Stem.Sig [76], resistance score [28], IPRES [36], ImmmunCells.Sig [77], T cell signature [23], immunosuppression Sig [78].

Potential cell-cell interactions explain the predictive performance of our random forest model

We aimed to further elucidate the effectiveness of our random forest model as the prognostic capabilities of this model have been demonstrated to be superior to that of T scores. The TiME of melanomas is shaped by both the composition of and spatial-temporal dynamics within the immune compartment [79,80], which may explain why the random forest model, capable of capturing associations between features (i.e., cell compositions), exhibits the best predictive performance. Hence, we sought to determine the correlations, in quantity and functionality, between different immune cell components within the melanoma TiME.

To this end, we first assessed for correlations among the abundances of the 36 different cell subtypes within the three single-cell transcriptomic datasets. We observed a positive correlation ($r = 0.74$, $p = 8.18e\text{-}18$) between the CD4-CXCL13 Tfh-like cell subtype, which exhibited significant weights in both the T score and random forest model, and the macrophage subtype (Macro-C1Q-TIMD4) (Fig. 5**A and B**), which is also enriched in melanoma patients resistant to immunotherapy (Fig. 5**C**). Further, Macro-C1Q-TIMD4 was identified as one of the terminally differentiated myeloid subtypes through calculating proliferation scores based on 3 genes (*MKI67, STMN1, KIAA0101*) identified in these cells (Fig. 5**D**). Moreover, the Macro-C1Q-TIMD4 subtype was predominantly present in ICB-resistant melanomas as well as was associated with tumor angiogenesis and complement activation (Fig. 5**D**).

We further investigated the molecular interactions between T-NK cells, myeloid cells, CD4-CXCL13 Tfh-like cells, and macro-C1Q-TIMD4 cells, with a particular focus on the latter two subtypes. Using the CellChat database [81], we found that the most abundant interactions occurred among myeloid subpopulations, suggesting the importance of myeloid interactions in shaping the TiME, as well as identified several interactions between myeloid and T-NK cells (Fig. 5**E**). We also investigated cytokine interactions between myeloid cells and T-NK cells and found that macro-C1Q-TIMD4 exhibits high expression of IL10 that shapes tumor immune suppressive environment, while lacking crucial cytokine signalings such as IL21 that are important for T cell development and survival. (Fig. 5**F**). Similar assessment of cytokine interactions between macro-C1Q-TIMD4 and CD4-CXCL13 Tfh-like subtypes revealed an upregulation of IL7 and IL10 signaling, which was then validated by ligand and receptor expression levels (Fig. 5**G–K**). IL10 signaling has been reported to be associated with CD4 T cell suppression and IL7 signaling is known to protect T cell from apoptosis [82,83]. Notably, IL7R is usually observed in naïve T cells and is critical for homeostatic proliferation and survival of naïve T cells [84]. Interestingly, we also observed a upregulation of IL7R in CD4-CXCL13 Tfh-like cells; these receptors may compete for IL7, which partially explain the relatively low naïve score for CD4 T cells from ICB-resistant melanomas (**Supplementary Fig. 3**). Activation of these signaling pathways is confirmed by increased activity of downstream JAK-STAT pathway, with the potential common target being the transcription factor STAT3 (**Supplementary Fig. 5**), which is widely recognized to be involved in tumor immune tolerance and tumor-promoting inflammation [85]. Taken together, these results suggest that the macro-C1Q-TIMD4 subtype may promote both the infiltration and survival of CD4-CXCL13 Tfh-like cells.

Discussion

While immunotherapeutics such as ICB have been shown to be effective against melanomas, the widely heterogenous response of melanoma patients to this mode of therapy has uncovered a need to develop patient-stratification tools for identifying those who will benefit most from ICB [86,87]. Here, we leverage transcriptomic data capturing the diversity and dynamics within the TiME to develop a predictive model for stratifying ICB-responsive and non-responsive melanoma patients. Specifically, we first constructed a predictive logistic regression model based on the composition of T cell populations within the melanoma TiME for predicting response of melanoma patients to ICB. This model exhibited a substantial capacity to differentiate between ICB-resistant and responsive melanomas as well as revealed CD4-CXCL13-Tfh cells as a potential predictive biomarker, which has not been reported for the prediction of melanoma immunotherapy. To increase the accuracy of our model, we incorporated transcriptomic data capturing the density and cell-cell interactions among all immune constituents within the melanoma TiME into a random forest model that demonstrated robust predictive performance across different datasets. Consistently, the pivotal roles of CD4-CXCL13 Tfh-like cells and CD8-CXCL13 T cells in our random forest model align with their functional significance in immunotherapy outcomes [68,73], thus confirming the importance of these cell subtypes in mediating response to treatment. Importantly, the predictive power of our random forest model was further validated in data from melanoma patients prior to ICB treatment [35–37] and shows a performance no less than other existing models, thus validating the translational potential of our model and suggesting that the TiME composition of treatment-naïve melanomas

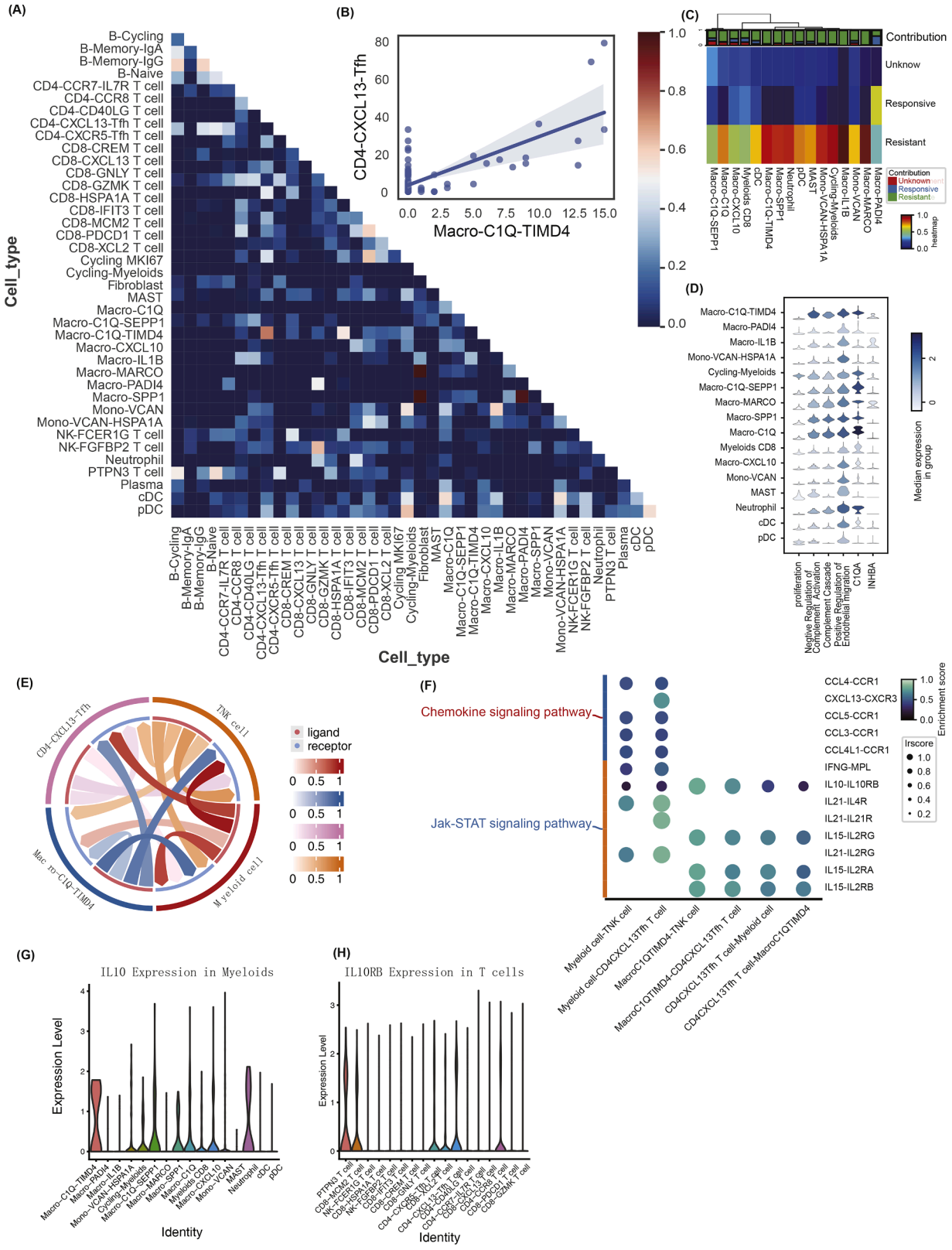

Fig 5. CD4+ CXCL13+ follicular helper T cells and C1Q+ TIMD4+ macrophages are positively correlated with tumor infiltration and explain the effectiveness of the model. (A) Pearson's correlation of cell fractions between different cell clusters. (B) Fraction of CD4+ CXCL13+ follicular helper T cells and C1Q+ TIMD4+ macrophages are positively correlated ($r = 0.74$, $p = 8.18e\text{-}18$). (C) Bar plot shows contribution of each condition to myeloid cell clusters. Heatmap shows cell fractions' average z-score for patients in each condition. (D) Swarm plot shows pathways and genes enriched in C1Q+ TIMD4+ macrophages. (E) Sankey plot shows interactions between T cell and myeloid cell clusters. Strength of interaction is indicated with more saturated colors. (F) Dot plot shows 13 enriched signaling pathways between T cell and myeloid cell clusters. (G and H) Expression levels of cytokine IL10 in myeloid cells (G) and its corresponding receptor IL10RB in T cells (H).

influences the patient response to ICB.

Consistent with other studies [28,88], the results of our analysis underscore the pivotal role of the TiME in determining the response of melanoma to ICB therapy. Specifically, we identified distinct differences in the composition of immune cell lineages between ICB-resistant and responsive melanoma tissues, with resistant tissues exhibiting an increased proportion of myeloid cells and CD8+ *T* cells and responsive tissues harboring components that enabled CD4+ *T* cell immunity. These findings align with previous reports [89–91], which have emphasized the importance of T cell populations in mediating the response to ICB therapy, as well as emphasize the dynamic nature of the T cell response to ICB therapy, which may explain the variability in response of melanoma patients.

Both our logistic regression and random forest models uncovered a central role for the CD4+ *T* cell subpopulations, specifically CD4+ CXCL13+ Tfh-like cells, in mediating resistance to ICB therapy in melanoma patients. Specifically, this T cell subtype exhibited a suppressive phenotype, with GO analysis revealing involvement in the negative regulation of T cell activation. Further, in line with previous research [92,93], CD4+ CXCL13+ Tfh-like cells shared similarities with Treg cells and conventional Tfh-like cells, thus indicating a potential for plasticity and functional diversity within this subset. Importantly, these cells were linked to the upregulation of immune escape-related genes, such as *CXCL13* and *TNFRSF4*, which are associated with poor prognosis in various cancer types [68,94–96]. Together, these findings underscore the need for a nuanced understanding of the specific T cell subsets and their functional implications within the TiME when developing models for guiding anti-cancer therapeutic strategies.

The higher predictive power of our random forest model when compared to our logistic regression model confirmed that immune constituents beyond the T cell compartment were involved in determining response of melanoma to ICB. Specifically, we found a positive correlation between CD4-CXCL13 Tfh cells and a macrophage subtype macro-C1Q-TIMD4, which is associated with reduced CD8+ *T* cell activity and relatively poor immune therapy responses [97–99]. This correlation suggests a potential mechanism through which these macrophages may influence the melanoma TiME and ultimately influence the effectiveness of immunotherapy.

Our study has certain limitations. To ensure the capture of rare cell subpopulations, we utilized all single-cell transcriptome data, including data from post-treatment patients, to construct predictive models for melanoma patient responses. This may introduce systematic biases into the predictive models. However, we validated the accuracy of our models by using three bulk RNA sequencing datasets from melanoma patients prior to ICB treatment, thus demonstrating that the effects of data contamination were limited. Furthermore, the comparison of changes in the TiME from pre-treatment to post-treatment may be leveraged to predict response of melanoma to immunotherapy. Additional studies are needed to understand the applicability of our models for tumor types beyond melanomas.

Conclusion

We have developed a highly accurate random forest model for predicting melanoma patient response to ICB intervention. Additionally, our data underscore the necessity of capturing the density and dynamics of all immune constituents within the TiME for developing predictive models. Our work contributes to the evolving landscape of precision medicine in melanoma, which emphasizes the importance of capturing the TiME to guide treatment decisions and improve patient outcomes. Future research efforts should focus on providing the clinical validation necessary to fully harness the potential of our model in a clinical setting as well as determine the applicability of our model for other tumor types.

Ethics approval and consent to participate

The datasets used in this research are all publicly available and do not require an ethics approval.

Consent for publication

The research does not involve participants. All of the authors agree with the publication of this research.

Availability of data and material

All of the data and computational algorithms used in this research is publicly available and the sources are correctly cited in the article.

CRediT authorship contribution statement

Yucheng Dong: Writing – original draft, Project administration, Methodology, Formal analysis, Conceptualization. **Zhizhuo Chen:** Writing – original draft, Project administration, Methodology, Formal analysis, Conceptualization. **Fan Yang:** Formal analysis, Data curation. **Jiaxin Wei:** Formal analysis, Data curation. **Jiuzuo Huang:** Writing – review & editing, Writing – original draft, Conceptualization. **Xiao Long:** Writing – review & editing, Writing – original draft, Formal analysis, Conceptualization.

Declaration of competing interest

The authors declare that they have no known competing financial interests or personal relationships that could have appeared to influence the work reported in this paper.

Acknowledgments

Yucheng Dong and Zhizhuo Chen contributed equally to this work

Supplementary materials

Supplementary material associated with this article can be found, in the online version, at doi:10.1016/j.tranon.2024.101910.

References

[1] D. Schadendorf, A.C. van Akkooi, C. Berking, K.G. Griewank, R. Gutzmer, A. Hauschild, A. Stang, A. Roesch, S. Ugurel, Melanoma, Lancet 392 (2018) 971–984.
[2] A.A. Albittar, O. Alhalabi, I.C. Glitza Oliva, Immunotherapy for melanoma, Immunotherapy (2020) 51–68.
[3] J.M. Kirkwood, A.A. Tarhini, M.C. Panelli, S.J. Moschos, H.M. Zarour, L. H. Butterfield, H.J. Gogas, Next generation of immunotherapy for melanoma, J. Clin. Oncol. 26 (2008) 3445–3455.
[4] F.S. Hodi, H. Kluger, M. Sznol, R. Carvajal, D. Lawrence, M. Atkins, J. Powderly, W. Sharfman, I. Puzanov, D. Smith, Abstract CT001: durable, long-term survival in previously treated patients with advanced melanoma (MEL) who received nivolumab (NIVO) monotherapy in a phase I trial, Cancer Res. 76 (2016) CT001. CT001.
[5] C. Robert, J. Schachter, G.V. Long, A. Arance, J.J. Grob, L. Mortier, A. Daud, M. S. Carlino, C. McNeil, M. Lotem, Pembrolizumab versus ipilimumab in advanced melanoma, N. Engl. J. Med. 372 (2015) 2521–2532.
[6] A.C. Huang, R. Zappasodi, A decade of checkpoint blockade immunotherapy in melanoma: understanding the molecular basis for immune sensitivity and resistance, Nat. Immunol. 23 (2022) 660–670.
[7] C. Trojaniello, M.G. Vitale, L. Scarpato, A. Esposito, P.A. Ascierto, Melanoma immunotherapy: strategies to overcome pharmacological resistance, Expert Rev. Anticancer Ther 20 (2020) 289–304.
[8] T.N. Gide, J.S. Wilmott, R.A. Scolyer, G.V. Long, Primary and acquired resistance to immune checkpoint inhibitors in metastatic melanoma, Clin. Cancer Res. 24 (2018) 1260–1270.
[9] J. Larkin, V. Chiarion-Sileni, R. Gonzalez, J.J. Grob, C.L. Cowey, C.D. Lao, D. Schadendorf, R. Dummer, M. Smylie, P. Rutkowski, Combined nivolumab and ipilimumab or monotherapy in untreated melanoma, N. Engl. J. Med. 373 (2015) 23–34.

[10] S.P. Patel, R. Kurzrock, PD-L1 expression as a predictive biomarker in cancer immunotherapy, Mol. Cancer Ther. 14 (2015) 847–856.
[11] T.A. Chan, M. Yarchoan, E. Jaffee, C. Swanton, S.A. Quezada, A. Stenzinger, S. Peters, Development of tumor mutation burden as an immunotherapy biomarker: utility for the oncology clinic, Ann. Oncol. 30 (2019) 44–56.
[12] L. Chang, M. Chang, H.M. Chang, F. Chang, Microsatellite instability: a predictive biomarker for cancer immunotherapy, Appl. Immunohistochem. Mol. Morphol. 26 (2018) e15–e21.
[13] D.P. Carbone, M. Reck, L. Paz-Ares, B. Creelan, L. Horn, M. Steins, E. Felip, M. M. van den Heuvel, T.E. Ciuleanu, F. Badin, et al., First-line nivolumab in stage IV or recurrent non-small-cell lung cancer, N. Engl. J. Med. 376 (2017) 2415–2426.
[14] Y. Takeuchi, A. Tanemura, Y. Tada, I. Katayama, A. Kumanogoh, H. Nishikawa, Clinical response to PD-1 blockade correlates with a sub-fraction of peripheral central memory CD4+ T cells in patients with malignant melanoma, Int. Immunol. 30 (2018) 13–22.
[15] B.P. Fairfax, C.A. Taylor, R.A. Watson, I. Nassiri, S. Danielli, H. Fang, E.A. Mahe, R. Cooper, V. Woodcock, Z. Traill, et al., Peripheral CD8(+) T cell characteristics associated with durable responses to immune checkpoint blockade in patients with metastatic melanoma, Nat. Med. 26 (2020) 193–199.
[16] S. Simon, V. Voillet, V. Vignard, Z. Wu, C. Dabrowski, N. Jouand, T. Beauvais, A. Khammari, C. Braudeau, R. Josien, et al., PD-1 and TIGIT coexpression identifies a circulating CD8 T cell subset predictive of response to anti-PD-1 therapy, J. Immunother. Cancer 8 (2020).
[17] R. Zappasodi, S. Budhu, M.D. Hellmann, M.A. Postow, Y. Senbabaoglu, S. Manne, B. Gasmi, C. Liu, H. Zhong, Y. Li, et al., Non-conventional inhibitory CD4(+)Foxp3(-)PD-1(hi) T cells as a biomarker of immune checkpoint blockade activity, Cancer Cell 34 (2018) 691.
[18] M. Binnewies, E.W. Roberts, K. Kersten, V. Chan, D.F. Fearon, M. Merad, L. M. Coussens, D.I. Gabrilovich, S. Ostrand-Rosenberg, C.C. Hedrick, Understanding the tumor immune microenvironment (TIME) for effective therapy, Nat. Med. 24 (2018) 541–550.
[19] W. Huang, Y. Jiang, W. Xiong, Z. Sun, C. Chen, Q. Yuan, K. Zhou, Z. Han, H. Feng, H. Chen, Noninvasive imaging of the tumor immune microenvironment correlates with response to immunotherapy in gastric cancer, Nat. Commun. 13 (2022) 5095.
[20] A. Hajiran, N. Chakiryan, A. Aydin, L. Zemp, J. Nguyen, J. Laborde, J. Chahoud, P. Spiess, S. Zaman, S. Falasiri, Reconnaissance of tumor immune microenvironment spatial heterogeneity in metastatic renal cell carcinoma and correlation with immunotherapy response, Clin. Exp. Immunol. 204 (2021) 96–106.
[21] X. Ren, L. Zhang, Y. Zhang, Z. Li, N. Siemers, Z. Zhang, Insights gained from single-cell analysis of immune cells in the tumor microenvironment, Annu. Rev. Immunol. 39 (2021) 583–609.
[22] T. Fu, L.J. Dai, S.Y. Wu, Y. Xiao, D. Ma, Y.Z. Jiang, Z.M. Shao, Spatial architecture of the immune microenvironment orchestrates tumor immunity and therapeutic response, J. Hematol. Oncol. 14 (2021) 98.
[23] M. Yan, J. Hu, Y. Ping, L. Xu, G. Liao, Z. Jiang, B. Pang, S. Sun, Y. Zhang, Y. Xiao, X. Li, Single-cell transcriptomic analysis reveals a tumor-reactive T cell signature associated with clinical outcome and immunotherapy response in melanoma, Front. Immunol. 12 (2021) 758288.
[24] Y. Ding, Z. Zhao, H. Cai, Y. Zhou, H. Chen, Y. Bai, Z. Liu, S. Liu, W. Zhou, Single-cell sequencing analysis related to sphingolipid metabolism guides immunotherapy and prognosis of skin cutaneous melanoma, Front. Immunol. 14 (2023) 1304466.
[25] J. Huuhtanen, H. Kasanen, K. Peltola, T. Lönnberg, V. Glumoff, O. Brück, O. Dufva, K. Peltonen, J. Vikkula, E. Jokinen, et al., Single-cell characterization of anti-LAG-3 and anti-PD-1 combination treatment in patients with melanoma, J. Clin. Investig. (2023) 133.
[26] P.H. Li, X.Y. Kong, Y.Z. He, Y. Liu, X. Peng, Z.H. Li, H. Xu, H. Luo, J. Park, Recent developments in application of single-cell RNA sequencing in the tumour immune microenvironment and cancer therapy, Mil Med. Res. 9 (2022) 52.
[27] I. Tirosh, B. Izar, S.M. Prakadan, M.H. Wadsworth, D. Treacy, J.J. Trombetta, A. Rotem, C. Rodman, C. Lian, G. Murphy, Dissecting the multicellular ecosystem of metastatic melanoma by single-cell RNA-seq, Science 352 (2016) 189–196.
[28] L. Jerby-Arnon, P. Shah, M.S. Cuoco, C. Rodman, M.J. Su, J.C. Melms, R. Leeson, A. Kanodia, S. Mei, J.R. Lin, A cancer cell program promotes T cell exclusion and resistance to checkpoint blockade, Cell 175 (2018) 984–997, e924.
[29] M. Sade-Feldman, K. Yizhak, S.L. Bjorgaard, J.P. Ray, C.G. de Boer, R.W. Jenkins, D.J. Lieb, J.H. Chen, D.T. Frederick, M. Barzily-Rokni, et al., Defining T cell states associated with response to checkpoint immunotherapy in melanoma, Cell 175 (2018) 998–1013, e1020.
[30] K. Lathrop, V. Kaklamani, The response evaluation criteria in solid tumors (RECIST), Predict. Biomark. Oncol. Appl. Precis. Med. (2019) 501–511.
[31] Y. Hao, S. Hao, E. Andersen-Nissen, W.M. Mauck, S. Zheng, A. Butler, M.J. Lee, A. J. Wilk, C. Darby, M. Zager, Integrated analysis of multimodal single-cell data, Cell 184 (2021) 3573–3587, e3529.
[32] F.A. Wolf, P. Angerer, F.J. Theis, SCANPY: large-scale single-cell gene expression data analysis, Genome Biol. 19 (2018) 1–5.
[33] I. Korsunsky, N. Millard, J. Fan, K. Slowikowski, F. Zhang, K. Wei, Y. Baglaenko, M. Brenner, P-r Loh, S. Raychaudhuri, Fast, sensitive and accurate integration of single-cell data with Harmony, Nat. Methods 16 (2019) 1289–1296.
[34] D. Combe, C. Largeron, M. Géry, Egyed-Zsigmond E: i-louvain: an attributed graph clustering method, in: Proceedings of the Advances in Intelligent Data Analysis XIV: 14th International Symposium, Springer, 2015, pp. 181–192. IDA 2015, Saint Etienne France, October 22-24, 2015 Proceedings 14.
[35] D. Liu, B. Schilling, D. Liu, A. Sucker, E. Livingstone, L. Jerby-Arnon, L. Zimmer, R. Gutzmer, I. Satzger, C. Loquai, Integrative molecular and clinical modeling of clinical outcomes to PD1 blockade in patients with metastatic melanoma, Nat. Med. 25 (2019) 1916–1927.
[36] W. Hugo, J.M. Zaretsky, L. Sun, C. Song, B.H. Moreno, S. Hu-Lieskovan, B. Berent-Maoz, J. Pang, B. Chmielowski, G. Cherry, Genomic and transcriptomic features of response to anti-PD-1 therapy in metastatic melanoma, Cell 165 (2016) 35–44.
[37] N. Riaz, J.J. Havel, V. Makarov, A. Desrichard, W.J. Urba, J.S. Sims, F.S. Hodi, S. Martín-Algarra, R. Mandal, W.H. Sharfman, Tumor and microenvironment evolution during immunotherapy with nivolumab, Cell 171 (2017) 934–949, e916.
[38] O. Bohnsack, A. Hoos, K. Ludajic, Adaptation of the immune related response criteria: irRECIST, Ann. Oncol. 25 (2014) iv369.
[39] F.A. Wolf, F.K. Hamey, M. Plass, J. Solana, J.S. Dahlin, B. Göttgens, N. Rajewsky, L. Simon, F.J. Theis, PAGA: graph abstraction reconciles clustering with trajectory inference through a topology preserving map of single cells, Genome Biol. 20 (2019) 1–9.
[40] K. Van den Berge, H. Roux de Bézieux, K. Street, W. Saelens, R. Cannoodt, Y. Saeys, S. Dudoit, L. Clement, Trajectory-based differential expression analysis for single-cell sequencing data, Nat. Commun. 11 (2020) 1201.
[41] A. Liberzon, A. Subramanian, R. Pinchback, H. Thorvaldsdóttir, P. Tamayo, J. P. Mesirov, Molecular signatures database (MSigDB) 3.0, Bioinformatics 27 (2011) 1739–1740.
[42] I.M.P. Badia, J. Velez Santiago, J. Braunger, C. Geiss, D. Dimitrov, S. Muller-Dott, P. Taus, A. Dugourd, C.H. Holland, R.O. Ramirez Flores, J. Saez-Rodriguez, decoupleR: ensemble of computational methods to infer biological activities from omics data, Bioinform. Adv. 2 (2022) vbac016.
[43] Y. Zhang, T. Liu, X. Hu, M. Wang, J. Wang, B. Zou, P. Tan, T. Cui, Y. Dou, L. Ning, CellCall: integrating paired ligand–receptor and transcription factor activities for cell–cell communication, Nucleic Acids Res. 49 (2021) 8520–8534.
[44] Y. Zhang, T. Liu, X. Hu, M. Wang, J. Wang, B. Zou, P. Tan, T. Cui, Y. Dou, L. Ning, et al., CellCall: integrating paired ligand-receptor and transcription factor activities for cell-cell communication, Nucleic Acids Res. 49 (2021) 8520–8534.
[45] C.B. Steen, C.L. Liu, A.A. Alizadeh, A.M. Newman, Profiling cell type abundance and expression in bulk tissues with CIBERSORTx, Stem Cell Transcr. Netw. Methods Protoc. (2020) 135–157.
[46] F. Pedregosa, G. Varoquaux, A. Gramfort, V. Michel, B. Thirion, O. Grisel, M. Blondel, P. Prettenhofer, R. Weiss, V. Dubourg, Scikit-learn: machine learning in Python, J. Mach. Learn. Res. 12 (2011) 2825–2830.
[47] T.G. Nick, K.M. Campbell, Logistic regression, Top. Biostat. (2007) 273–301.
[48] M.A. Hearst, S.T. Dumais, E. Osuna, J. Platt, B. Scholkopf, Support vector machines, IEEE Intell. Syst. Appl. 13 (1998) 18–28.
[49] Berrar D.: Bayes' theorem and naive Bayes classifier. Encyclopedia of Bioinformatics and Computational Biology: ABC of Bioinformatics 2018, 403:412.
[50] A. Natekin, A. Knoll, Gradient boosting machines, a tutorial, Front. Neurorobot. 7 (2013) 21.
[51] Qi Y.: Random forest for bioinformatics. Ensemble Machine Learning: Methods and Applications 2012:307–323.
[52] D.A. Van Dyk, X.L. Meng, The art of data augmentation, J. Comput. Graph. Stat. 10 (2001) 1–50.
[53] A.M. Newman, C.B. Steen, C.L. Liu, A.J. Gentles, A.A. Chaudhuri, F. Scherer, M. S. Khodadoust, M.S. Esfahani, B.A. Luca, D. Steiner, et al., Determining cell type abundance and expression from bulk tissues with digital cytometry, Nat. Biotechnol. 37 (2019) 773–782.
[54] A. Xia, Y. Zhang, J. Xu, T. Yin, X.J. Lu, T cell dysfunction in cancer immunity and immunotherapy, Front. Immunol. 10 (2019) 1719.
[55] M. Terranova-Barberio, N. Pawlowska, M. Dhawan, M. Moasser, A.J. Chien, M. E. Melisko, H. Rugo, R. Rahimi, T. Deal, A. Daud, Exhausted T cell signature predicts immunotherapy response in ER-positive breast cancer, Nat. Commun. 11 (2020) 3584.
[56] C. Zhang, J. Li, Y. Cheng, F. Meng, J.W. Song, X. Fan, H. Fan, J. Li, Y.L. Fu, M. J. Zhou, et al., Single-cell RNA sequencing reveals intrahepatic and peripheral immune characteristics related to disease phases in HBV-infected patients, Gut 72 (2023) 153–167.
[57] R. Zappasodi, I. Serganova, I.J. Cohen, M. Maeda, M. Shindo, Y. Senbabaoglu, M. J. Watson, A. Leftin, R. Maniyar, S. Verma, et al., CTLA-4 blockade drives loss of T (reg) stability in glycolysis-low tumours, Nature 591 (2021) 652–658.
[58] S. Tietscher, J. Wagner, T. Anzeneder, C. Langwieder, M. Rees, B. Sobottka, N. de Souza, B. Bodenmiller, A comprehensive single-cell map of T cell exhaustion-associated immune environments in human breast cancer, Nat. Commun. 14 (2023) 98.
[59] M. Hinterbrandner, V. Rubino, C. Stoll, S. Forster, N. Schnüriger, R. Radpour, G. M. Baerlocher, A.F. Ochsenbein, C. Riether, Tnfrsf4-expressing regulatory T cells promote immune escape of chronic myeloid leukemia stem cells, JCI Insight 6 (2021).
[60] X. Lin, L. Ye, X. Wang, Z. Liao, J. Dong, Y. Yang, R. Zhang, H. Li, P. Li, L. Ding, et al., Follicular helper T cells remodel the immune microenvironment of pancreatic cancer via secreting CXCL13 and IL-21, Cancers 13 (2021) (Basel).
[61] Y. Xia, Y. Wang, Y. Hao, M. Shan, H. Liu, Z. Liang, Multi-omics integrative analysis reveals the role of tumor necrosis factor superfamily member 4 in keloidal scarring, Am. J. Transl. Res. 15 (2023) 1607–1625.
[62] J. Sprent, C.D. Surh, Normal T cell homeostasis: the conversion of naive cells into memory-phenotype cells, Nat. Immunol. 12 (2011) 478–484.
[63] J. Vent-Schmidt, J.M. Han, K.G. MacDonald, M.K. Levings, The role of FOXP3 in regulating immune responses, Int. Rev. Immunol. 33 (2014) 110–128.
[64] M. Diupotex, J. Zamora-Chimal, J.A. Gajón, L.C. Bonifaz, I. Becker, CXCR5 and TIM-3 expressions define distinct exhausted T cell subsets in experimental cutaneous infection with Leishmania mexicana, Front. Immunol. (2023) 14.

[65] C. Levelt, M. Van Oostendorp, Feature co-occurrence constraints in L1 acquisition, Linguist. Neth. 24 (2007) 162–172.
[66] E. Ahn, K. Araki, M. Hashimoto, W. Li, J.L. Riley, J. Cheung, A.H. Sharpe, G. J. Freeman, B.A. Irving, R. Ahmed, Role of PD-1 during effector CD8 T cell differentiation, Proc. Natl. Acad. Sci. U. S. A. 115 (2018) 4749–4754.
[67] J. Yeong, J.C.T. Lim, B. Lee, H. Li, C.C.H. Ong, A.A. Thike, W.H. Yeap, Y. Yang, A.Y. H. Lim, T.K.Y. Tay, et al., Prognostic value of CD8 + PD-1+ immune infiltrates and PDCD1 gene expression in triple negative breast cancer, J. Immunother. Cancer 7 (2019) 34.
[68] X. Lin, L. Ye, X. Wang, Z. Liao, J. Dong, Y. Yang, R. Zhang, H. Li, P. Li, L. Ding, Follicular helper T cells remodel the immune microenvironment of pancreatic cancer via secreting CXCL13 and IL-21, Cancers 13 (2021) 3678 (Basel).
[69] S. Kalaora, A. Nagler, J.A. Wargo, Y. Samuels, Mechanisms of immune activation and regulation: lessons from melanoma, Nat. Rev. Cancer 22 (2022) 195–207.
[70] M. Marzagalli, N.D. Ebelt, E.R. Manuel, Unraveling the crosstalk between melanoma and immune cells in the tumor microenvironment, Semin. Cancer Biol. 59 (2019) 236–250.
[71] Y. Cheng, Y. Si, L. Wang, M. Ding, S. Yu, L. Lu, Y. Guo, M. Zong, L. Fan, The regulation of macrophage polarization by hypoxia-PADI4 coordination in Rheumatoid arthritis, Int. Immunopharmacol. 99 (2021) 107988.
[72] A.H. Jonsson, F. Zhang, G. Dunlap, E. Gomez-Rivas, G.F. Watts, H.J. Faust, K. V. Rupani, J.R. Mears, N. Meednu, R. Wang, Granzyme K+ CD8 T cells form a core population in inflamed human tissue, Sci. Transl. Med. 14 (2022) eabo0686.
[73] H.H. Workel, J.M. Lubbers, R. Arnold, T.M. Prins, P. van der Vlies, K. de Lange, T. Bosse, I.C. van Gool, F.A. Eggink, M.C.A. Wouters, et al., A transcriptionally distinct CXCL13+CD103+CD8+ T-cell population is associated with B-cell recruitment and neoantigen load in human cancer, Cancer Immunol. Res. 7 (2019) 784–796.
[74] S. Kobayashi, T. Watanabe, R. Suzuki, M. Furu, H. Ito, J. Ito, S. Matsuda, H. Yoshitomi, TGF-β induces the differentiation of human CXCL13-producing CD4 + T cells, Eur. J. Immunol. 46 (2016) 360–371.
[75] N. Auslander, G. Zhang, J.S. Lee, D.T. Frederick, B. Miao, T. Moll, T. Tian, Z. Wei, S. Madan, R.J. Sullivan, et al., Robust prediction of response to immune checkpoint blockade therapy in metastatic melanoma, Nat. Med. 24 (2018) 1545–1549.
[76] Z. Zhang, Z.X. Wang, Y.X. Chen, H.X. Wu, L. Yin, Q. Zhao, H.Y. Luo, Z.L. Zeng, M. Z. Qiu, R.H. Xu, Integrated analysis of single-cell and bulk RNA sequencing data reveals a pan-cancer stemness signature predicting immunotherapy response, Genome Med. 14 (2022) 45.
[77] D. Xiong, Y. Wang, M. You, A gene expression signature of TREM2hi macrophages and γδ T cells predicts immunotherapy response, Nat. Commun. 11 (2020) 5084.
[78] C. Cui, C. Xu, W. Yang, Z. Chi, X. Sheng, L. Si, Y. Xie, J. Yu, S. Wang, R. Yu, et al., Ratio of the interferon-γ signature to the immunosuppression signature predicts anti-PD-1 therapy response in melanoma, NPJ Genom. Med. 6 (2021) 7.
[79] G. Imparato, F. Urciuolo, C. Mazio, P.A. Netti, Capturing the spatial and temporal dynamics of tumor stroma for on-chip optimization of microenvironmental targeting nanomedicine, Lab. Chip 23 (2023) 25–43.
[80] S.K. Longo, M.G. Guo, A.L. Ji, P.A. Khavari, Integrating single-cell and spatial transcriptomics to elucidate intercellular tissue dynamics, Nat. Rev. Genet. 22 (2021) 627–644.
[81] S. Jin, C.F. Guerrero-Juarez, L. Zhang, I. Chang, R. Ramos, C.H. Kuan, P. Myung, M. V. Plikus, Q. Nie, Inference and analysis of cell-cell communication using CellChat, Nat. Commun. 12 (2021) 1088.
[82] D.G. Brooks, K.B. Walsh, H. Elsaesser, M.B. Oldstone, IL-10 directly suppresses CD4 but not CD8 T cell effector and memory responses following acute viral infection, Proc. Natl. Acad. Sci. 107 (2010) 3018–3023.
[83] N. Chetoui, M. Boisvert, S. Gendron, F. Aoudjit, Interleukin-7 promotes the survival of human CD4+ effector/memory T cells by up-regulating Bcl-2 proteins and activating the JAK/STAT signalling pathway, Immunology 130 (2010) 418–426.
[84] F. Carrette, C.D. Surh, IL-7 signaling and CD127 receptor regulation in the control of T cell homeostasis. Seminars in Immunology, Elsevier, 2012, pp. 209–217.
[85] S. Zou, Q. Tong, B. Liu, W. Huang, Y. Tian, X. Fu, Targeting STAT3 in cancer immunotherapy, Mol. Cancer 19 (2020) 145.
[86] Y. Lei, X. Li, Q. Huang, X. Zheng, M. Liu, Progress and challenges of predictive biomarkers for immune checkpoint blockade, Front. Oncol. 11 (2021) 617335.
[87] S. Arora, R. Velichinskii, R.W. Lesh, U. Ali, M. Kubiak, P. Bansal, H. Borghaei, M. J. Edelman, Y. Boumber, Existing and emerging biomarkers for immune checkpoint immunotherapy in solid tumors, Adv. Ther. 36 (2019) 2638–2678.
[88] H. Li, A.M. van der Leun, I. Yofe, Y. Lubling, D. Gelbard-Solodkin, A.C. van Akkooi, M. van den Braber, E.A. Rozeman, J.B. Haanen, C.U. Blank, Dysfunctional CD8 T cells form a proliferative, dynamically regulated compartment within human melanoma, Cell 176 (2019) 775–789, e718.
[89] I.S. Kim, Y. Gao, T. Welte, H. Wang, J. Liu, M. Janghorban, K. Sheng, Y. Niu, A. Goldstein, N. Zhao, et al., Immuno-subtyping of breast cancer reveals distinct myeloid cell profiles and immunotherapy resistance mechanisms, Nat. Cell Biol. 21 (2019) 1113–1126.
[90] M.F. Sanmamed, X. Nie, S.S. Desai, F. Villaroel-Espindola, T. Badri, D. Zhao, A. W. Kim, L. Ji, T. Zhang, E. Quinlan, A burned-out CD8+ T-cell subset expands in the tumor microenvironment and curbs cancer immunotherapy, Cancer Discov. 11 (2021) 1700–1715.
[91] R.E. Tay, E.K. Richardson, H.C. Toh, Revisiting the role of CD4(+) T cells in cancer immunotherapy-new insights into old paradigms, Cancer Gene Ther. 28 (2021) 5–17.
[92] M. Ukita, J. Hamanishi, H. Yoshitomi, K. Yamanoi, S. Takamatsu, A. Ueda, H. Suzuki, Y. Hosoe, Y. Furutake, M. Taki, et al., CXCL13-producing CD4+ T cells accumulate in the early phase of tertiary lymphoid structures in ovarian cancer, JCI Insight (2022) 7.
[93] M. Cohen, A. Giladi, O. Barboy, P. Hamon, B. Li, M. Zada, A. Gurevich-Shapiro, C. G. Beccaria, E. David, B.B. Maier, The interaction of CD4+ helper T cells with dendritic cells shapes the tumor microenvironment and immune checkpoint blockade response, Nat. Cancer 3 (2022) 303–317.
[94] S. Wu, R. Sun, B. Tan, B. Chen, W. Zhou, D.S. Gao, J. Zhong, H. Huang, J. Jiang, B. Lu, The half-life-extended IL21 can be combined with multiple checkpoint inhibitors for tumor immunotherapy, Front. Cell Dev. Biol. 9 (2021) 779865.
[95] Y. Hu, J. Liu, J. Yu, F. Yang, M. Zhang, Y. Liu, S. Ma, X. Zhou, J. Wang, Y. Han, Identification and validation a costimulatory molecule gene signature to predict the prognosis and immunotherapy response for hepatocellular carcinoma, Cancer Cell Int. 22 (2022) 97.
[96] H. Ma, P.H. Feng, Yu S-n, Z.H. Lu, Q. Yu, J. Chen, Identification and validation of TNFRSF4 as a high-profile biomarker for prognosis and immunomodulation in endometrial carcinoma, BMC Cancer 22 (2022) 543.
[97] A. Chow, S. Schad, M.D. Green, M.D. Hellmann, V. Allaj, N. Ceglia, G. Zago, N. S. Shah, S.K. Sharma, M. Mattar, Tim-4+ cavity-resident macrophages impair anti-tumor CD8+ T cell immunity, Cancer Cell 39 (2021) 973–988, e979.
[98] J. Li, S.Y. Kim, N.M. Lainez, D. Coss, M.G. Nair, Macrophage-regulatory T cell interactions promote type 2 immune homeostasis through resistin-like molecule α, Front. Immunol. 12 (2021) 710406.
[99] X. Zheng, X. Wang, X. Cheng, Z. Liu, Y. Yin, X. Li, Z. Huang, Z. Wang, W. Guo, F. Ginhoux, Single-cell analyses implicate ascites in remodeling the ecosystems of primary and metastatic tumors in ovarian cancer, Nat. Cancer 4 (2023) 1138–1156.